Article

Single molecule tracking based drug screening

Daisuke Watanabe [1,2], Michio Hiroshima [1,2] ✉, Masato Yasui [3] &
Masahiro Ueda [1,2,4] ✉

The single-molecule tracking of transmembrane receptors in living cells has
provided significant insights into signaling mechanisms, such as mobility and
clustering upon their activation/inactivation, making it a potential screening
method for drug discovery. Here we show that single-molecule tracking-based
screening can be used to explore compounds both detectable and undetect-
able by conventional methods for disease-related receptors. Using an auto-
mated system for a fast large-scale single-molecule analysis, we screen for
epidermal growth factor receptor (EGFR) from 1134 of FDA approved drugs.
The 18 hit compounds include all EGFR-targeted tyrosine kinase inhibitors
(TKIs) in the library that suppress any phosphorylation-dependent mobility
shift of EGFR, proving the concept of this approach. The remaining hit com-
pounds are not reported as EGFR-targeted drugs and do not inhibit EGF-
induced EGFR phosphorylation. These non-TKI compounds affect the mobility
and/or clustering of EGFR without EGF and induce EGFR internalization,
to impede EGFR-dependent cell growth. Thus, single-molecule tracking
provides an alternative modality for discovering therapeutics on various
receptor functions with previously untargeted mechanisms.

Transmembrane receptors trigger signal transduction to induce cel-
lular responses. Since the downstream signaling depends on the
functional properties of receptors, various diseases are often attrib-
uted to receptor dysfunction. In drug discovery, the largest number of
target molecules are membrane receptors (>50% of total), such as
receptor tyrosine kinases (RTKs), G protein-coupled receptors
(GPCRs), and immune receptors, followed by nuclear receptors
(<20%)[1–3]. Epidermal growth factor receptor (EGFR), an RTK, mediates
signal transduction for cell proliferation, differentiation, migration,
and apoptosis, and is a primary target molecule in drug exploration
because its overexpression and/or mutations are found in various
types of cancer cells[4–7]. Many small-molecule drugs against a well-
known EGFR-related cancer, non-small cell lung cancer (NSCLC), have
been developed: gefitinib, erlotinib, and icotinib as first-generation
tyrosine kinase inhibitors (TKIs); afatinib and dacomitinib as second-

generation TKIs; and osimertinib as third-generation[8]. These drugs
have been evaluated by their inhibitory effects on tyrosine kinase
activity[9], but EGFR undergoes multiple signaling processes including
tyrosine phosphorylation, oligomerization, coupling with adapter
molecules, and internalization on the membrane of living cells[10]. Dis-
turbing these processes can affect the signaling activity of the mole-
cule, providing a potential mechanistic target for drug discovery. In
general, assays for drug discovery focus on a particular step in the
signaling pathway exhibited by the targeted molecules. However,
assays that select for compounds that have effects on multiple steps in
the signaling pathway are of interest because of their different
mechanisms of action on the same target[11].

Single-molecule imaging analysis has been used to visualize and
measure the location and brightness of individual membrane receptor
molecules in cells[12–14]. These measurements provide information on

[1]Laboratory of Single Molecule Biology, Graduate School of Frontier Biosciences, Osaka University, Suita, Osaka, Japan. [2]Laboratory for Cell Signaling
Dynamics, Center for Biosystems Dynamics Research, RIKEN, Suita, Osaka, Japan. [3]ZIDO Corporation, Toyonaka, Osaka, Japan. [4]Department of Biological
Sciences, Graduate School of Science, Osaka University, Toyonaka, Osaka, Japan. ✉e-mail: m_hiroshima.fbs@osaka-u.ac.jp;
ueda.masahiro.fbs@osaka-u.ac.jp

the lateral diffusion and oligomerization/clustering of receptors on the membrane of living cells. In the case of EGFR, the behavioral transition on the membrane, which is described by EGFR mobility and clustering dynamics, has been shown to correlate to the signaling process[15–19]: EGF triggers tyrosine phosphorylation, leading to the translocation of EGFR along the membrane to a specific region where the mobility of EGFR is confined and the clusters responsible for downstream signaling are formed, followed by internalization into endosomes. Single-molecule imaging has also revealed other processes during EGFR signaling, such as ligand-receptor binding kinetics, molecular structure transitions depending on membrane components, and colocalization with receptors for different signaling pathways. That is, single-molecule imaging has the potential to elucidate the effects of pharmacological compounds on multiple events during a series of EGFR signaling processes. In particular, this technique can detect changes in the physical properties of the target receptor, which include the lateral diffusion and the statistical distribution of receptor clusters, both of which are difficult to detect using biochemical methods. However, the low throughput of single-molecule imaging for data acquisition, which arises from its expertize- and manual-dependent workflow, prevents this method from being employed for large-scale single-molecule analysis. As a solution, we previously achieved a fully automated, in-cell single-molecule imaging system equipped with robotics and machine learning (AiSIS)[20,21] that has a 100-fold higher throughput than standard single-molecule analysis techniques. High-throughput analysis by AiSIS enables the evaluation of numerous compounds by detecting their effect on molecular mobility and clustering during the signaling process, which provides a form of molecular-targeted drug screening.

Here, we report a single-molecule tracking-based technique for the screening of compounds targeting transmembrane receptors. The successful selection of all TKIs for EGFR from a library consisting of 1134 FDA-approved compounds provides the proof of concept of this approach. The other hit compounds exhibit effects on the clustering, internalization, and expression level of EGFR without strong inhibition of the tyrosine kinase activity upon EGF stimulation. Unlike screening methods that focus on a single event in the molecular process, our method can assess various physical events at the single-molecule level occurring during the signal transduction of the target molecule.

Results

### EGFR mobility-based screening

AiSIS allows for a large-scale, single-molecule analysis of plasma membrane receptors using 96-well plates (Fig. 1a). Cells in each well were treated with a compound, and single-molecule imaging using total internal reflection fluorescence microscopy (TIRFM) was automatically executed well by well. Autofocusing mechanism (Fig. 1b and Supplementary Fig. 1) kept the in-focus position precise to acquire high magnification images of living cells with clear single fluorescence spots of the target molecules on the membrane by TIRFM. The fields of view suitable for the single-molecule analysis were determined by machine learning-based automated cell searching (Supplementary Movie 1). During the imaging, autofocusing was continuously running, and the ligand was dispensed at desired times by robotics. In the case of measuring 20 cells under one measurement condition, as described later, 480 different measurement conditions for ligand/compound concentrations, time of the addition, and duration of the treatment could be examined on demand in a single assay in one day. By observing individual cells under uniform fluorescence excitation at high magnification, quantitative analysis of the position as well as the fluorescence intensity of the fluorescent spots is possible, which allows the characterization of not only the lateral mobility of the target molecule but also the cluster formation of the target molecule. Figure 1c and Supplementary Movie 2a show a single EGFR-mEGFP complex expressed in CHO-K1 cells, which lack endogenous EGFR. From

the images acquired under optimized conditions, trajectory data, including the positions and brightness of fluorescent EGFR, were obtained by single-molecule tracking (Fig. 1d) and used to quantify the mobility of EGFR with diffusion coefficients and mean square displacements (MSD) (Fig. 1e). The mobility decreased with EGF addition, as shown by the MSD (Fig. 1f), consistent with a previous study[20]. This EGF-induced mobility shift was recovered by treatment with a TKI (gefitinib; Fig. 1e, bottom, and Supplementary Movie 2b), which confirmed EGFR mobility tightly correlated with EGF-activated kinase function. As shown in Fig. 1f, a linear relationship was found between the MSD for 500 ms (MSD_{500ms}) and EGFR phosphorylation under various EGF concentrations. Both data were obtained approximately 2 min after EGF addition, a time that represents the early phase of EGFR signaling just after reaching maximum EGFR phosphorylation. The inhibitory effect of gefitinib on the EGF-induced decrease of MSD_{500ms} is shown in Fig. 1g (top). Because TKI itself seems to have little effect on the mobility in our data, the MSD ratio (MSD with EGF to MSD without EGF) was used to evaluate the compounds en bloc. As shown in Fig. 1g (bottom), when the EGF concentration was 30 nM, the ratio was approximately 0.2 for TKI-untreated cells but approached 1 for treated cells due to suppression of the EGF-induced decrease of EGFR mobility.

We extended the single-molecule tracking-based assay to drug screening. First, we optimized the conditions of the image acquisition (Supplementary Fig. 2), and the suitability of this approach as a screening method was assessed using the indices calculated from MSD_{500ms}, with the positive control being cells treated with gefitinib and EGF and the negative control being cells treated only with EGF (Fig. 2a). The coefficient of variation (CV), signal/background (S/B), and Z'-factor were respectively defined as the ratio of the standard deviation (SD) and average of the controls, the ratio between the averages of the positive (signal) and negative (background) controls, and the following equation:

$$Z' = 1 - \left(3 \times SD_{positive} + 3 \times SD_{negative}\right) / \left(Avg_{positive} - Avg_{negative}\right) \quad (1)$$

where $SD_{positive}$, $SD_{negative}$, $Avg_{positive}$, and $Avg_{negative}$ represent the SD and average for the positive and negative controls, respectively. The obtained indices for our system were 6% for CV, 6.2 for S/B, and 0.69 for Z'-factor. All these values were shown to satisfy the thresholds of ≤ 10% for CV, ≥2 for SB, and ≥ 0.50 for Z'-factor for drug screening (Supplementary Table 1). Next, we carried out the screening using a library of 1134 FDA-approved compounds whose target proteins are responsible for broad functions such as receptors, channels, kinases, enzymes, transporters, and so on (Fig. 2b, Supplementary Table 2, and Supplementary Data 1). This library includes 7 marketed drugs that act as TKI for EGFR (afatinib, erlotinib, OSI-420 (the active metabolite of erlotinib), gefitinib, lapatinib, lapatinib ditosylate (another form of lapatinib), and vandetanib). To explore compounds significantly affecting EGFR mobility, the screening procedure was designed as follows: 1) cultured cells in each well of a 96-well plate were pretreated with 100 μL of 10 μM compound solution at 37 °C for 1 h, 2) single-molecule imaging was automatically done on 20 different cells, 3) 100 μL of 120 nM EGF solution was added by the automatic dispenser so that the final concentration of EGF was 60 nM, and 4) another 20 cells were imaged 2 min after the EGF addition. During the screening, the Z'-factor was calculated for every assay plate from positive- and negative control wells (20 cells in each well) to evaluate the screening quality and images acquired from the plates passing the quality inspection were used in the following analysis (Supplementary Fig. 3a). To achieve a highly accurate screening, $MSD_{\Delta t}$ was determined for every plate with the time duration (Δt) that provides the highest Z'-factor. For each compound, when the $MSD_{\Delta t}$ ratio was beyond the average +3 SD of the $MSD_{\Delta t}$ ratio for the negative control, the compound was regarded as causing a
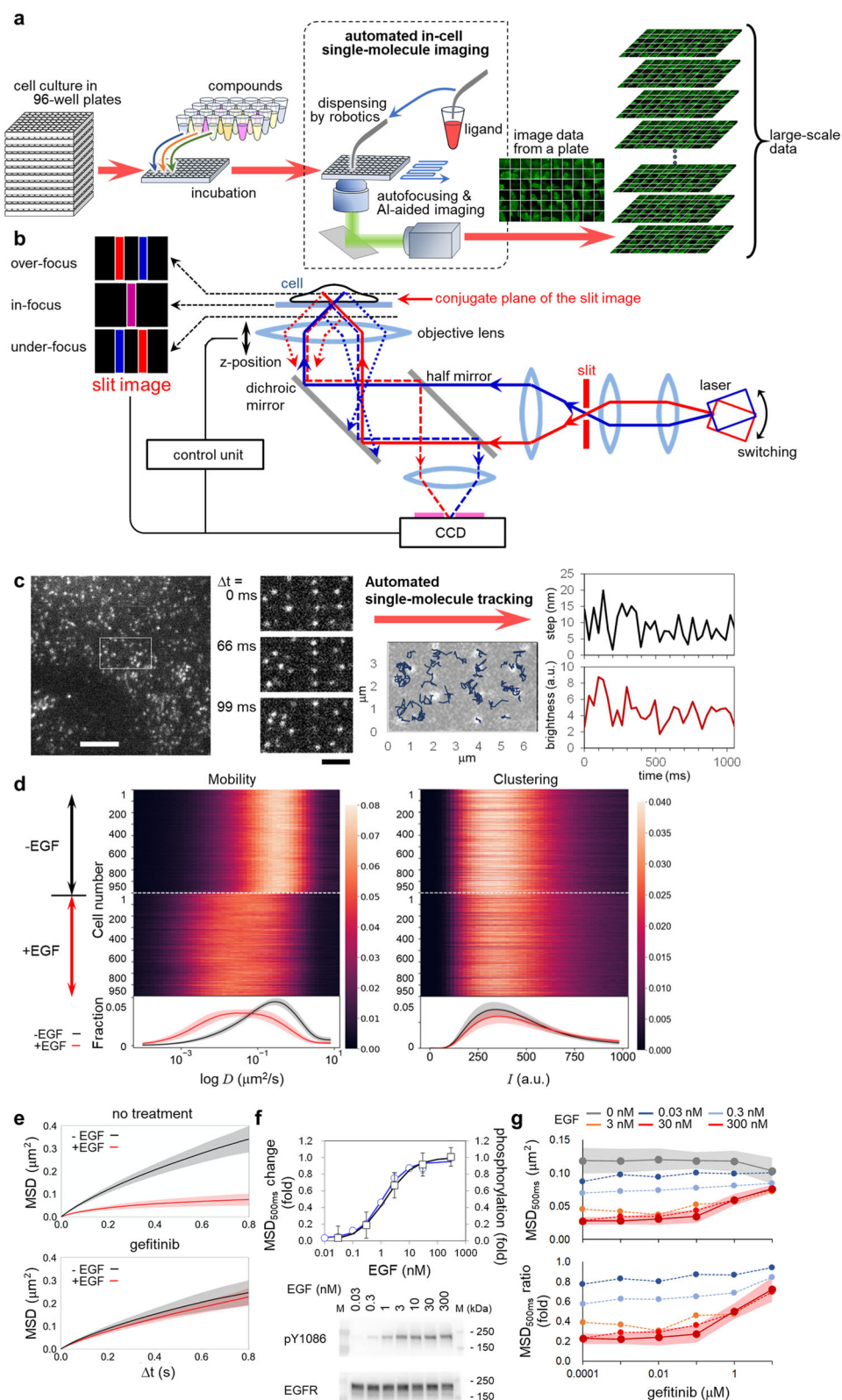
significant MSD change of EGFR and identified as a hit compound. Figure 2c shows the selected 53 compounds with $MSD_{\Delta t}$ ratios for compounds normalized to the negative control ratio. One of the marketed EGFR-targeted drugs, genistein, which is a flavonoid and known to inhibit tyrosine kinases including EGFR, was excluded due to its IC_{50} (50% inhibitory concentration) being above 10 μM, which was beyond our experimental condition.

For a more detailed assessment of the selected 53 compounds, we measured the dose-dependent effects of the compounds on EGFR mobility with and without EGF (Supplementary Fig. 4 and Supplementary Data 2). Compounds with significantly different MSD values at the minimum and maximum concentrations were selected. When half of the difference between the MSD (averaged over ~30 cells) at the two concentrations exceeded the sum of their SD, the compound was

Fig. 1 | Large-scale single-molecule imaging analysis of fluorescently labeled EGFR for drug screening. a Schematic flow of single-molecule imaging using AiSIS for drug screening. **b** Optics of the autofocus device. Slit images, which reflect deviation from the in-focus position of the objective lens, are generated with switching illumination and used for feedback control. **c** Automated single-molecule tracking. Left, representative images of EGFR-mEGFP observed with AiSIS. Scale bar, 5 μm. Middle left, time series images of the squared region in the left panel. Scale bar, 2 μm. Representative images obtained by single-molecule imaging are displayed. Middle right, trajectories of EGFR (>8 frames). Right, time series of step length (top) and brightness (bottom) of a spot in the left panels. **d** Heatmaps of diffusion coefficients and brightness measured before and 5 min after the EGF addition. The average distributions over the cells are shown at the bottom. Black and red lines with shaded areas indicate the average with SD before and after EGF addition, respectively. **e** Time development of MSDs (mean square displacements)

for either untreated or gefitinib-treated (10 μM for 1 hour) cells without (black) and with EGF (300 nM, red). The acquisition of single-molecule images began 1 min after the EGF addition. Data are from 60 cells for each condition (Supplementary Table 3). **f** Relative changes in MSD_{500ms} and fold changes of phosphorylation obtained from western blotting (bottom) against different EGF concentrations. Single-molecule imaging and the phosphorylation assay began 1 and 2 min after the EGF addition, respectively. Data of MSD and phosphorylation are from 140 cells and 7 independent experiments, respectively, for each EGF concentration. M indicates molecular weight marker. **g** Dose-dependency of gefitinib on MSD. Top, MSD versus gefitinib concentration. Bottom, ratios between MSD with and without EGF. Colored curves correspond to the indicated EGF concentrations. Single-molecule imaging began 1 min after the EGF addition. Data are from 33 cells for each concentration. Shaded areas (**d**, **e**, and **g**) and error bars (**f**) indicate the SD and SE around the mean, respectively. Source data are provided as a Source Data file.

regarded as a hit compound. As a result, 18 compounds were obtained, but one of them, auranofin, was excluded from further analysis due to its cytotoxicity (cell death) during the treatment. Although these compounds showed similarly high MSD ratios, we found two types of effects on the MSD: one changed the receptor mobility primarily after the EGF addition (Fig. 2d), and the other before the addition (Fig. 2e). Among the 17 compounds, 10 compounds corresponded to the former case and suppressed the EGF-dependent decrease in a dose-dependent manner (Fig. 2d). These 10 were all kinase inhibitors: afatinib, erlotinib, OSI-420, gefitinib, lapatinib, and lapatinib ditosylate are known as EGFR-TKIs[8,22]; ponatinib and vandetanib are pan-TKIs[23]; and dasatinib and ibrutinib have been reported as Bruton's tyrosine kinase inhibitors[24] and can interfere with EGFR phosphorylation. All these EGFR-TKIs in the library were hit compounds (Supplementary Data 1), proving that our method was valid for exploring drugs targeting tyrosine phosphorylation of the receptor.

The other 7 hit compounds did not affect the EGF-induced decrease in mobility of EGFR but did affect the mobility without EGF stimulation (Fig. 2e). The reported drug actions and approved applicable symptoms are not apparently concerned with EGFR tyrosine kinases: broxyquinoline is an anti-infective-agent; daunorubicin is an anthracycline antibiotic used for chemotherapeutic agents against cancer by inhibiting DNA topoisomerase II[25]; eltrombopag is used to treat severe aplastic anemia and activates thrombopoietin receptor (TPOR) to facilitate platelet production[26]; glafenine is a non-steroidal anti-inflammatory drug (NSAID) that inhibits cyclooxygenase-2/prostaglandin E2 (COX-2/PGE2) signaling[27]; nilotinib and sorafenib are not EGFR-TKI but TKI that largely inhibit EGFR-independent pathways and used respectively to treat primary kidney cancer[28] and chronic myeloid leukemia[29]; and, finally, curcumin interferes with tyrosine kinases including EGFR and is approved as a food additive. Because these compounds induced EGFR mobility changes without EGF, they are suggested to interact directly or indirectly with EGFR by some actions other than the inhibition of tyrosine kinase. The effects of these compounds on EGFR are described in more detail below.

EGFR clustering-based screening

Single-molecule tracking can obtain the brightness of each EGFR-mEGFP fluorescent spot, which reflects the number of fluorescent GFP involved. Uniform illumination was required to quantify the brightness. AiSIS achieved uniform TIR illumination over 3000 μm². Because CHO-K1 cells express no endogenous EGFR, their brightness typically reflects the oligomer/clustering size. The EGF concentration correlated with the brightness (Fig. 3a and b), indicating that monomers/dimers were relatively reduced with increasing concentration, and larger size clusters were gained. The formation of clusters with integrating monomers/dimers has been suggested to correlate with the activation of downstream signaling through interactions with adapter molecules[15]. Thus, the increase in

brightness could be used as a screening index to assess signal transduction.

For the obtained single-molecule tracking data, we compared the probability density distributions of the spot brightness before and after compound treatment without EGF. The Kullback–Leibler divergence (KLD) was used to quantify the similarity of the histogram profiles. In this case, Z'-factors were calculated using KLD before and after the EGF addition (without any compound) as respective negative and positive controls. The observed Z'-factors did not satisfy the threshold of 0.5 due to the broad SD (Supplementary Fig. 3b). Nevertheless, the highest KLD value among the compounds (Fig. 3c) was obviously different from the KLD calculated for the negative control. This compound, verteporfin, diminished the number of brighter spots in a dose-dependent manner (Fig. 3d–f), suggesting that larger clusters of EGFR decreased on the plasma membrane. Verteporfin reduced EGFR diffusion in a dose-dependent manner without EGF, although it was not selected from the mobility-based screen due to its modest effects (Fig. 3g). Verteporfin is a photosensitizing drug for age-related macular degeneration[30]. As described in more detail below, the effect of this compound on EGFR was due to EGFR internalization and not to any photophysical effect.

Characterization of hit compounds on EGFR dynamics, signal transduction, and cell viability

To determine whether these non-EGFR-TKI compounds affect EGFR-dependent signaling in CHO-K1 cells expressing EGFR, which were used in the screening, we examined the activation and expression levels of both EGFR and the downstream signaling protein ERK (Fig. 4a–c). Treatment with any of five non-EGFR-TKI compounds (broxyquinoline, daunorubicin, eltrombopag, sorafenib, and verteporfin) caused no significant inhibition of EGFR phosphorylation upon EGF stimulation in comparison with the control (compound-untreated) condition (Fig. 4a and b, left), a finding consistent with these compounds not being EGFR-TKIs. In the subsequent signaling, the phosphorylation of ERK fell upon treatment with any of the five compounds, especially eltrombopag, sorafenib, and verteporfin, although the expression levels of ERK were not affected, indicating an inhibition of EGFR-dependent signaling (Fig. 4a and b, right). The total amount of EGFR was decreased by treatment with the five compounds (Fig. 4c) regardless of EGF stimulation, indicating the destabilization of EGFR. Furthermore, EGFR was internalized in the cells treated with the five compounds without EGF, as shown in timelapse TIRF images (Fig. 4d and Supplementary movie 3) and by quantification (Fig. 4e). In the case of verteporfin, the photoreactive damage of GFP induced by repetitive laser irradiation was observed because of the photosensitizing effect of verteporfin (Supplementary Fig. 5a). Further observations of EGFR-mEGFP at the condition minimizing the photophysical effects suggested EGFR internalization (Fig. 4d, e, and Supplementary Fig. 5b, c). The examination by immunofluorescence microscopy of verteporfin supported EGFR internalization, as
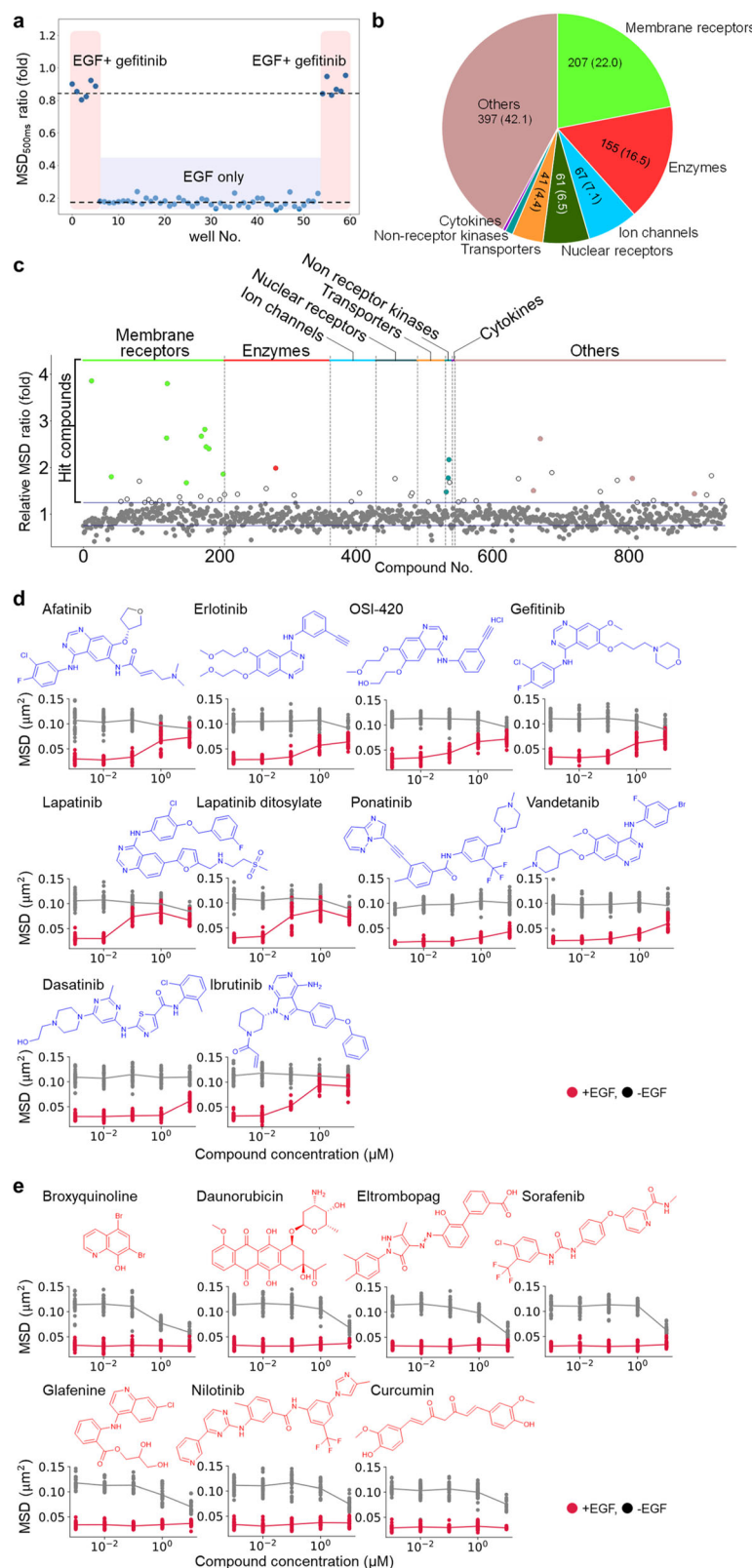
described later. In contrast with these five non-EGFR-TKI compounds, when treated with the other two compounds, glafenine and nilotinib, the cells exhibited no reduction of EGF-induced EGFR phosphorylation or downstream ERK (Fig. 4b) and showed no obvious internalization or degradation of EGFR (Fig. 4c and e). Thus, the five non-EGFR-TKI compounds (broxyquinoline, daunorubicin, eltrombopag, sorafenib, and verteporfin) caused the downregulation of EGFR-related signal

transduction with internalization, even though EGFR phosphorylation was unchanged. That is, compounds that can alter EGFR signaling outside tyrosine phosphorylation were successfully selected by the single-molecule tracking-based screening method.

We next evaluated the effects of the hit compounds on EGFR-dependent cellular viability by utilizing various cell types that express EGFR because they are expected to depend on EGFR signaling for their

Fig. 2 | EGFR mobility-based screening for compounds in an FDA-approved library. a Evaluation of single-molecule tracking as a screening method. MSD_{500ms} ratios of EGFR were calculated with and without gefitinib as positive and negative controls, respectively. Red-shaded regions indicate the MSD_{500ms} ratio obtained from wells treated with 30 nM EGF and gefitinib (positive control), and the blue-shaded region indicates wells treated with only EGF (negative control). Single-molecule imaging began 1 minute after EGF addition. **b** Target proteins of FDA-approved compounds in the library. **c** Effects of compounds on EGFR mobility were evaluated using the $MSD_{\Delta t}$ ratio in which Δt provided optimal duration to obtain the best Z'-factor value in each well plate (Supplementary Fig. 3a). Ratios for compound-treated cells were normalized to that for untreated cells. Blue lines denote upper and lower thresholds. The 53 hit compounds beyond the upper threshold are indicated by the colored and white circles. After further evaluation, the selected 18 compounds were denoted by colored circles, in which the colors indicate the type of target protein. **d, e** The dose-dependency was further evaluated by referring MSD_{167ms} against a series of compound concentrations. Red and black circles denote MSD values with and without EGF, respectively. 10 compounds (except auranofin) suppressed the EGF-dependent decrease in MSD (**d**), and 7 compounds reduced MSD regardless of the EGF concentration (**e**). Source data are provided as a Source Data file.
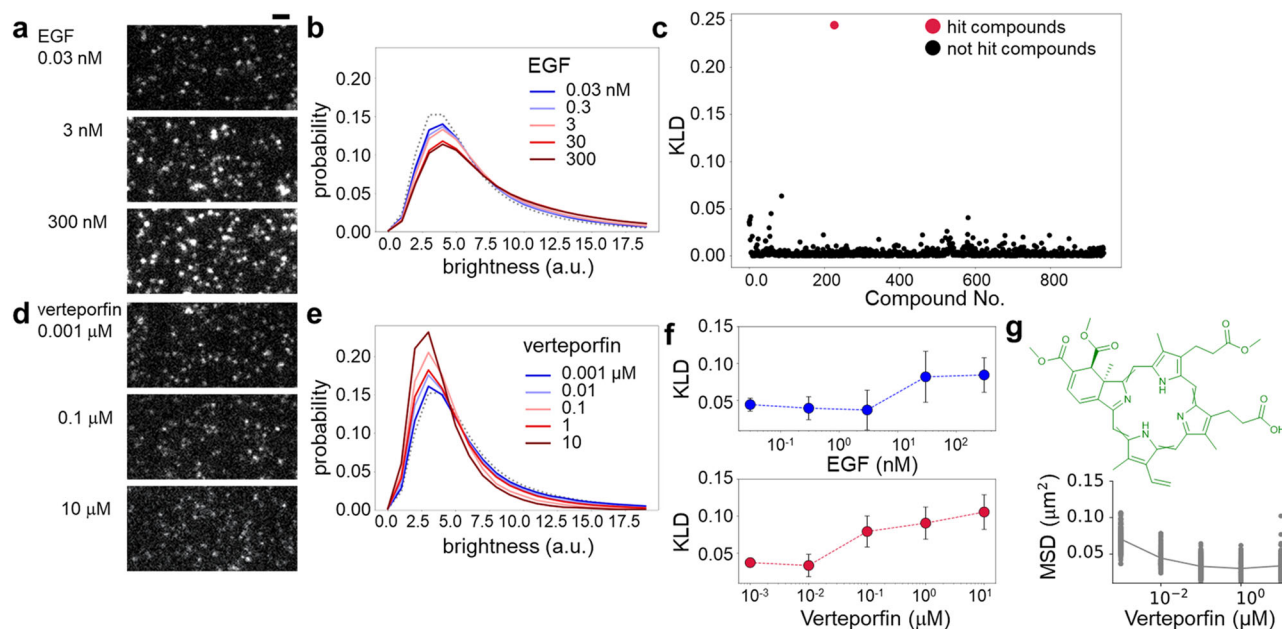
Fig. 3 | EGFR clustering-based screening for compounds in the FDA-approved library. a EGF facilitated the formation of EGFR oligomers. Single-molecule images of EGFR showed brighter and larger fluorescent spots were increased as the EGF concentration increased. Single-molecule imaging began 1 min after the EGF addition. Scale bar, 2 μm. **b** The probability distribution of EGFR spot brightness. EGFR fractions shifted from small to large oligomers with higher EGF concentrations. **c** Effects of compounds on EGFR oligomerization were evaluated using the KLD (Kullback–Leibler divergence) of the brightness histograms before and after the compound treatment. Verteporfin exhibited high KLD values (red dot). **d** Verteporfin treatment increased the EGFR spots with lower brightness. **e** The probability distribution of EGFR spot brightness. The fraction of smaller EGFR oligomers was increased with verteporfin concentration, suggesting disassembly of the EGFR oligomers. **f** EGF (top), and verteporfin (bottom) dose-dependent KLD against the untreated condition. Data are presented as the mean ± SD from 4 independent experiments. **g** The dose-dependency was further evaluated by referring to MSD_{167ms} for verteporfin. Black circles denote MSD values without EGF, showing the reduction of MSD without EGF. Representative images from 4 independent experiments are displayed (**a, d**). Source data are provided as a Source Data file.

survival: A431 and HeLa cells, which express endogenous EGFR, and EGFR-transfected Ba/F3 cells. We also utilized Ba/F3 and CHO-K1 cells, which do not express EGFR, as controls. Viability assays were carried out under 10 μM of compound for 72 h. The left panel in Fig. 5a shows that all hit EGFR-TKIs (i.e., afatinib, erlotinib, gefitinib, lapatinib, ponatinib, vandetanib, dasatinib and ibrutinib) reduced the viability of A431 cells and EGFR-transfected Ba/F3 cells, consistent with a dependency on EGFR activity for their survival[31,32]. HeLa cells, which expressed EGFR 10-fold less than A431 cells[33], also exhibited less viability with EGFR-TKI treatment, although they were somehow resistant to erlotinib and gefitinib, consistent with previous reports[34–36]. Similar to the effects of most EGFR-TKIs, the five non-EGFR-TKI compounds (broxyquinoline, daunorubicin, eltrombopag, sorafenib, and verteporfin) suppressed the viability of the three EGFR-expressing cell types, while the other two non-EGFR-TKIs (glafenine and nilotinib) caused higher viability. In the right panel in Fig. 5a, the viability of CHO-K1 and Ba/F3 cells was not significantly suppressed by EGFR-TKIs or the five non-EGFR-TKI compounds. These observations indicate that the five non-EGFR-TKI compounds suppress EGFR-dependent cell survival.

The viability of CHO-K1 cells lacking EGFR expression was sensitive to ponatinib and dasatinib, possibly due to these compounds acting as TKIs for other tyrosine kinases as well as EGFR.

We further evaluated the effects of the five non-EGFR-TKI compounds on EGFR signaling in the various cell lines. The EGF-induced phosphorylation of EGFR was observed with the non-EGFR-TKI compounds in A431, HeLa, and EGFR-transfected Ba/F3 cells (Fig. 5b and Supplementary Fig. 6), although at varying degrees, especially for verteporfin. The expression level of EGFR tended to be reduced slightly by the five compounds in A431 and EGFR-transfected Ba/F3 cells but rarely in HeLa cells (Fig. 5c). Verteporfin, in particular, caused EGFR-destabilization in EGFR-transfected Ba/F3 cells, which can explain the reduced EGF-induced EGFR phosphorylation (Fig. 5b).

The stability and internalization of EGFR were further examined in the EGFR-expressing cell lines by immunofluorescence microscopy, in which the photophysical effect of verteporfin need not be considered. Treatment with any of the five non-EGFR-TKI compounds caused a decrease in EGFR localization on the membrane in A431, HeLa, and EGFR-transfected Ba/F3 cells compared to untreated cell lines (Fig. 5d).
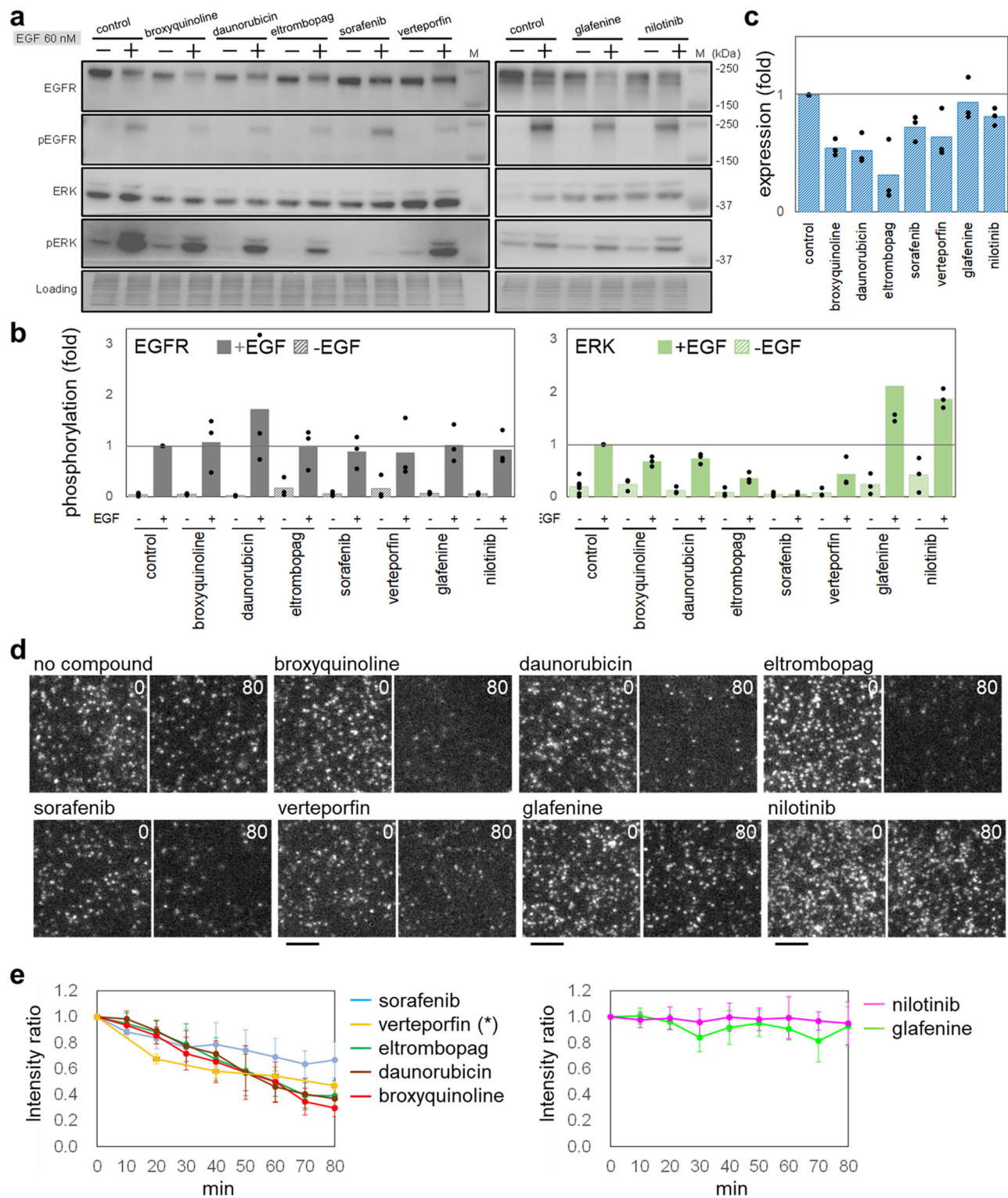
Fig. 4 | Effects of compounds on EGFR behavior and cell responses. Phosphorylation of EGFR and its downstream signaling protein (**a**, **b**) and EGFR protein expression in CHO-K1 cells expressing EGFR (**c**). After treatment with the indicated compounds for 1 h (dashed bar), the cells were stimulated with EGF for 5 min (filled bar). Band densities were normalized to the EGF-stimulated (**b**) and unstimulated (**c**) conditions. Gray lines indicate phosphorylation and expression levels in untreated cells. M indicates molecular weight marker, and representative images from 3 independent experiments are displayed (**a**). **d** Timelapse single-molecule images acquired at 0 and 80 min after the compound treatment. Scale bar, 3 μm. Representative images from 11 independent experiments are displayed.

e Quantified fluorescence per unit area, which was normalized to that at time 0. Solid lines correspond to the indicated compound. Timelapse images were acquired at the denoted time points in the same cells except verteporfin (*) for which the images were obtained at two-time points (0 and the other) to avoid the fluorescence bleaching induced by multiple laser irradiation. Data are presented as mean ± SD. n = 56, 61, 72, 47, 63, 42, and 46 cells from 5, 5, 6, 5, 9, 4, and 4 independent experiments for broxyquinoline, daunorubicin, eltrombopag, sorafenib, verteporfin, glafenine, and nilotinib, respectively. Source data are provided as a Source Data file.
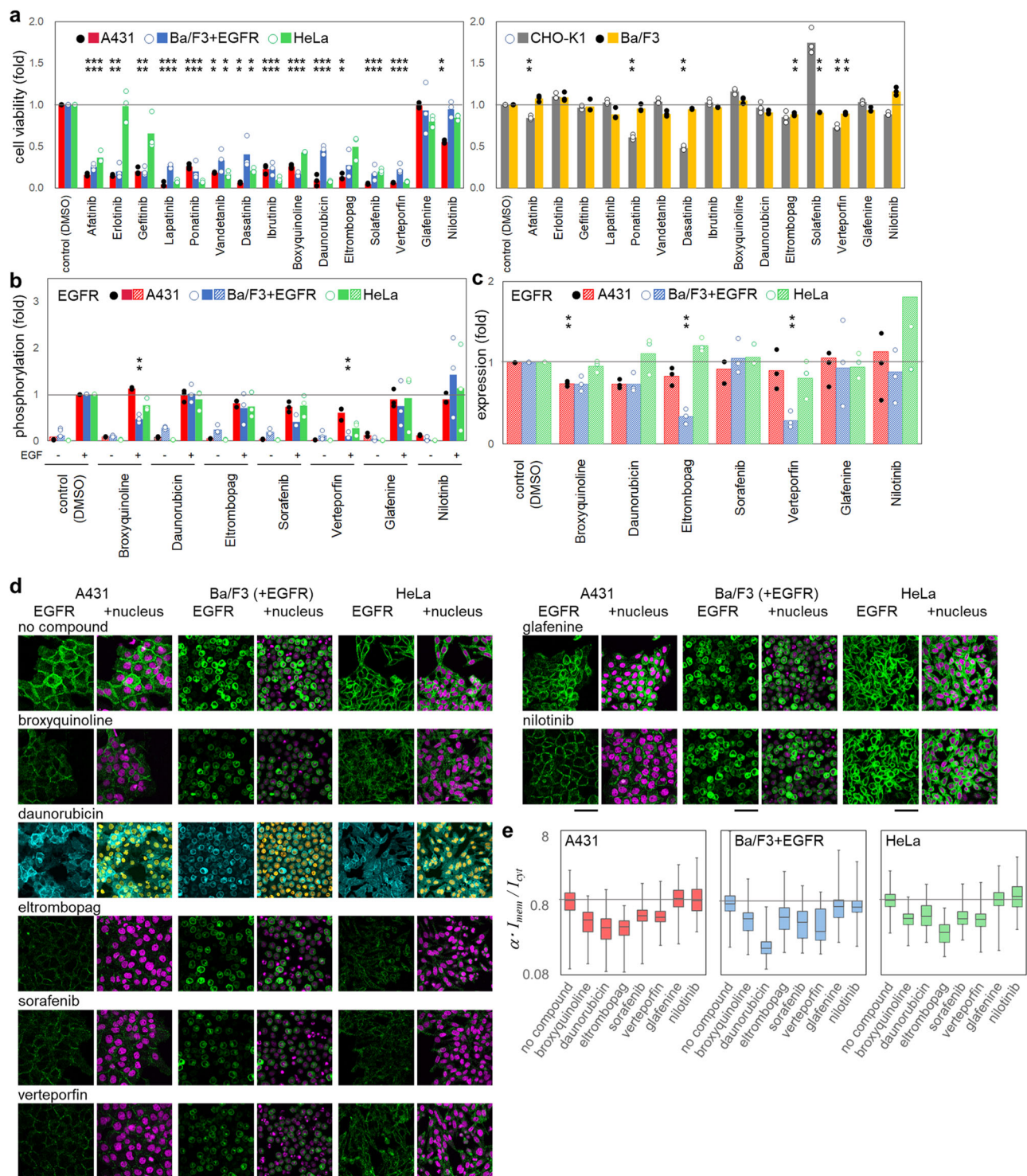
In particular, eltrombopag, sorafenib, and verteporfin tended to decrease the total expression level of EGFR, suggesting the internalization and degradation of EGFR. Figure 5e shows the ratio of EGFR localization on the plasma membrane and in the cytoplasm of the EGFR-positive cell lines treated with the non-EGFR-TKI compounds, revealing the five compounds enhanced the internalization of EGFR. In contrast, the other two compounds (glafenine and nilotinib) did not alter EGFR-dependent cell viability (Fig. 5a), EGF-induced EGFR phosphorylation (Fig. 5b), the expression level of EGFR (Fig. 5c), or the membrane localization of EGFR (Fig. 5d and e), indicating no effects on EGFR-dependent signaling or cell survival, although these compounds affected EGFR mobility (Fig. 2e). Thus, the hit compounds, which were

selected using EGFR-expressing CHO-K1 cells, were confirmed to robustly exert inhibitory effects on the EGFR-dependent cell viability by inducing the internalization and degradation of EGFR in various cell types including A431, EGFR-transfected Ba/F3, and Hela cells, albeit to varying degrees.

Overall, the hit EGFR-TKIs that inhibited the phosphorylation-dependent mobility shift of EGFR reduced the EGFR-dependent viability. The five non-EGFR-TKI compounds (broxyquinoline, daunorubicin, eltrombopag, sorafenib, and verteporfin) that decreased EGFR diffusion or clusters without EGF, reduced EGFR-dependent cell viability by downregulating EGFR. In contrast, the other two non-EGFR-TKI compounds (glafenine and nilotinib) that affected EGFR mobility

Fig. 5 | Effects of compounds on different cell lines. a Viabilities of cell lines treated with the hit compounds including EGFR-TKIs. Left, EGFR-expressing cell lines: A431 (red), EGFR-transfected Ba/F3 (light blue), and HeLa (green). Right, non-EGFR-expressing cell lines: CHO-K1 (gray) and Ba/F3 (orange). Viabilities were normalized to those of compound-untreated control cells. Asterisks indicate significant differences from control (**$p < 0.01$; two-sided Welch's t-test, Supplementary Table 4). **b, c** Phosphorylation of EGFR (**b**), which was normalized by that in cells after EGF stimulation, and EGFR protein expression (**c**), which was normalized by that in cells before the stimulation. Compound treatment was carried out with the indicated compounds for 1 h (dashed bar), and cells were subsequently stimulated with EGF for 2 min (filled bar). Gray lines indicate phosphorylation and expression levels in compound-untreated cells. Asterisks indicate significant differences from control (**$p < 0.01$; two-sided Welch's t-test, Supplementary Table 4). **d** Immuno-fluorescent images of EGFR in A431, Ba/F3 expressing EGFR, and HeLa cells acquired at 1 h after the compound treatment. Each cell was recognized by its nucleus. Because daunorubicin has an auto-fluorescence in the nucleus at 488 nm excitation, EGFR was observed using a second antibody at 640 nm excitation. For the other compounds, EGFR was observed at 488 nm excitation (see "Methods"). Scale bar, 100 μm. Representative images from 6 independent experiments are displayed. **e** Internalization was quantified using the average fluorescence intensities of the plasma membrane and cytoplasm regions ($\alpha \cdot I_{mem}/I_{cyt}$, see "Methods"). Values were normalized to that of untreated cells (gray lines). The box-and-whisker plots show the median as horizontal lines, the first and third quartiles as box ends, and the whiskers as minimum and maximum values. Data for broxyquinoline, daunorubicin, eltrombopag, sorafenib, verteporfin, glafenine, and nilotinib were respectively acquired from 332, 326, 177, 402, 476, 282, 454, and 363 A431 cells; 562, 406, 322, 422, 446, 564, and 506 BaF3 cells expressing EGFR; and 466, 321, 220, 353, 302, 363, 643, and 496 HeLa cells. Source data are provided as a Source Data file.
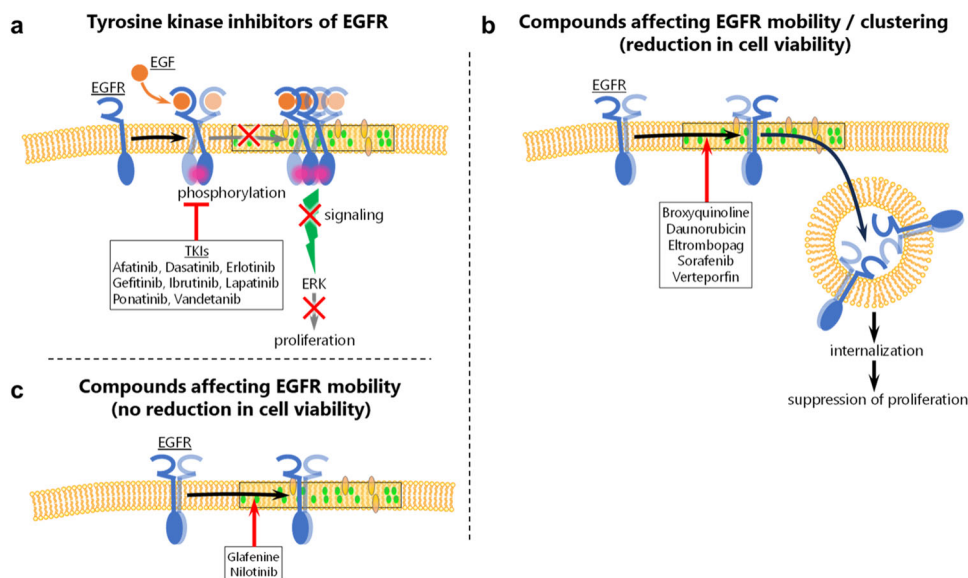
Fig. 6 | Categorized schemes for effects of hit compounds on EGFR. Observed schemes of the hit compounds. **a** TKIs suppress the EGF-induced phosphorylation of EGFR, thereby inhibiting the subsequent signaling process. **b** Compounds reducing both EGFR mobility and clustering induce EGFR internalization. **c** The internalization of EGFR was not observed in cells treated with compounds that reduced EGFR mobility but not cell viability (glafenine and nilotinib).

without EGF stimulation did not affect the EGFR-dependent signaling needed for cell survival.

Discussion

Here, we demonstrated single-molecule tracking-based drug screening to explore compounds effective against EGFR. In addition to the methods used in previous single-molecule screening for nuclear receptors[37], AiSIS enabled highly precise auto-focusing on the plasma membrane receptor and uniform TIR illumination for the quantification of fluorescence brightness. Our method observed changes in EGFR mobility and clustering instead of focusing on a specific process of the signaling, allowing it to detect changes in multiple processes dependent on the ligand. Because changes in the mobility and cluster distribution of the target molecule can hardly be measured by biochemical methods but can be observed by single-molecule imaging as signaling processes, our single-molecule tracking-based screening has the potential to detect compounds that cannot be detected by conventional methods. Screening by assessing several treatment conditions of ligand/compound led to a wide selection of compounds affecting EGFR functions that are related or unrelated to EGF stimulation (Fig. 2). Among the hit compounds, those suppressing the EGF-induced mobility shift of EGFR were identified as EGFR-TKIs, proving the reliability of the method for drug screening. One of the possible reasons why EGFR-targeted TKIs can be detected by mobility-based

screening is described in Fig. 6a. Accumulating evidence shows that EGFR undergoes structural changes during its phosphorylation upon EGF stimulation and then translocates to a confined membrane region via interactions with membrane components (lipid, proteins, etc.), leading to slower receptor mobility[15]. Changes in the MSD of EGFR were proven to couple tightly with the phosphorylation in a dose-dependent manner (Fig. 1f). The competitive docking of TKI to the ATP-binding pocket of EGFR prevents the receptor from subsequent structural changes during phosphorylation, which thus suppresses the decrease in mobility and subsequent signaling processes.

In addition to the detection of EGFR-TKIs, our screening detected non-EGFR-TKI compounds (i.e., broxyquinoline, daunorubicin, eltrombopag, sorafenib, verteporfin, glafenine, and nilotinib), none of which are known to act on EGFR directly. Figure 6b illustrates a scheme for the broxyquinoline, daunorubicin, eltrombopag, sorafenib, and verteporfin effects; these compounds commonly reduced mobility, induced internalization, decreased the expression levels of EGFR, and affected EGFR-dependent signaling and viability. We assume that these compounds force EGFR to a specific membrane subdomain where receptor mobility is lower. EGFR in the membrane subdomains may internalize via caveolin-mediated endocytosis[38,39]. The internalization exerts a harmful effect on cell viability by suppressing EGFR signaling for proliferation and survival[40]. For example, oxidative processes in cells are induced by various compounds (e.g., broxyquinoline) and

have been suggested to affect EGFR signaling[41]. Previous studies have shown that broxyquinoline stabilizes hypoxia-inducible factor (HIF) −1[42] to accumulate caveolin-1 in the lipid raft to constitute caveolae[43], which directly interacts with EGFR, suggesting the confined mobility and internalization of the protein complex including EGFR. In fact, we confirmed that broxyquinoline increased HIF-1 and the internalization of EGFR with caveolin in EGFR-transfected CHO-K1 cells (Supplementary Fig. 7). Furthermore, some compounds may induce complex formation including EGFR, thereby promoting the internalization and degradation of EGFR[38,44,45]. In addition, some compounds are reported to interact with the plasma membrane to possibly alter EGFR mobility[46,47]. Figure 6c illustrates the case of glafenine and nilotinib. No significant change was observed in the EGFR-dependent viability of cells treated by these two compounds (Fig. 5). Additionally, the phosphorylation of downstream proteins was not suppressed, and no internalization/reduction of EGFR expression occurred (Figs. 4 and 5), indicating no downregulation of EGFR signaling by these two compounds.

As described above, the hit compounds obtained in the present study were categorized into three types based on the observed EGFR behavior and cell responses, with each type suggested to depend on a different mechanism of action. The scheme in Fig. 6a, which illustrates that EGFR-TKIs can be obtained by the mobility-based screening, is useful for searching for effective TKIs if EGFR mutants resistant to existing TKIs appear to change their motility upon EGF-stimulated activation[48]. The scheme in Fig. 6b, which was suggested from the five non-EGFR-TKI compounds, is effective for removing pathogenic cells that excessively express EGFR, a common phenotype of various cancers, by inducing cell death following EGFR internalization. Therefore, drug repositioning for EGFR drugs may be possible using compounds that exhibit this scheme. In Fig. 6c, compounds that do not significantly affect cell viability but exert an effect on receptor mobility might be drug seeds with little cytotoxicity. Besides EGFR, various types of receptors on the plasma membrane have been reported to change their mobility according to their activation and the cluster formation to propagate downstream signaling[15,37,49], suggesting that single-molecule tracking-based drug screening is applicable to a wide variety of membrane receptors.

Methods
Cell preparation
CHO-K1, A431, and HeLa cells (RIKEN BRC through the National Bio-Resource Project of the MEXT, Japan) were grown at 37 °C in Ham's F-12 medium (CHO-K1) or Dulbecco's modified Eagle's medium (A431, HeLa; DMEM, FUJIFILM Wako Pure Chemical, Japan); both media were supplemented with 10% fetal bovine serum (FBS). Ba/F3 cells (RIKEN BRC) and Ba/F3 cells expressing EGFR[50,51] (a kind gift from Dr. Ryo Iwamoto and Dr. Eisuke Mekata, Osaka University) were cultured at 37 °C in RPMI medium supplemented with 10% FBS and 4 ng/mL mouse IL3 (091-03971, Fuji-Wako, Japan). In the case of Ba/F3 cells expressing EGFR, 20 ng/mL EGF (315-09, PeproTech, USA) was added to the medium. The culture medium was replaced with DMEM minus phenol red or FBS for starvation two hours before single-molecule imaging when the medium was changed to DMEM containing 5 mM PIPES. The cells were cultured until 90% confluence and observed in 60 wells of a 96-well plate (GP96000, Matsunami Glass, Japan); the peripheral wells were excluded to avoid interference between the microscope stage and the objective lens.

A stable CHO-K1 cell line expressing EGFR-mEGFP with an appropriate molecular density (1–3 μm^{-2}) on the basal membrane was established for single-molecule tracking. A DNA construct linking the cDNA of human EGFR (Supplementary Data 3, provided by Akihiko Yoshimura, Keio University) to the pEGFP-C1 vector (Clontech, Japan) was transfected to parental CHO-K1 cells with 80% confluency in a 6 cm dish using FuGENE HD (Promega, USA) with 2 μg of the construct mixed with 500 μL of OptiMEM (31985-062, Gibco, USA). A fraction of cells expressing EGFR-mEGFP was collected using a SH800S cell sorter (Sony, Japan) 2–3 days after the transfection. By sorting with a 488 nm laser, cells exhibiting a higher fluorescence intensity than the auto-fluorescence measured beforehand were selected and isolated. Cell cloning was carried out using the limiting dilution method, and the expression level of EGFR-mEGFP was confirmed for each clone using TIRFM by determining if individual fluorescent spots were distinguishable. When the expression level of EGFR-mEGFP was considerably increased during the passage, the cell sorting and cloning process were executed again to supply the appropriate cells to single-molecule imaging. AI-aided cell-searching was applied to the imaging to acquire images of cells with a suitable molecular density of 0.76 ± 0.55 μm^{-2}.

Automated in-cell single-molecule imaging system (AiSIS)
AiSIS consists of an automated microscope for single-molecule imaging and robotics for liquid dispensing. Total internal reflection (TIR) illumination was configurable with a high-magnification objective, PlanApo 60X NA 1.49 (Nikon, Japan), to acquire single-molecule images at the basal cell surface under an inverted microscope (Ti2-E, Nikon, Japan). Auto Imaging System (ZIDO Corp., Japan), including an autofocus device and AI-aided cell searching applications, was equipped to automatically obtain in-focus images of the cells with a suitable density of fluorescent spots for single-molecule analysis. Lasers at wavelengths of 488 nm (OBIS 488LS, Coherent, USA) were used to excite GFP fused with EGFR. The dichroic mirror/emission filter set was DM495/BA500-545 (Nikon, Japan). The images were acquired at a frame rate of 33 ms for 25 frames using a sCMOS camera (ORCA-Flash4.0 V2, Hamamatsu, Japan). A liquid-handling robot (Cavro Omni Robot, Tecan, USA) automatically sucked 100 μL of two-fold the final concentration of EGF solution from the well in the storage plate and dispensed the solution into the target well of the cell culture plate with 100 μL of observation medium.

Autofocus device
The device consists of a light source, magnifier optics, a slit located at the plane optically conjugated to the basal cell surface, a CCD camera for acquiring the slit image, and a control unit that feedback-controls the position of the objective lens (Fig. 1b). An 830 nm laser is used as the light source, and its incident angle is switched between two values using a Galvano mirror with a frequency of 10 Hz. The slit image on the CCD is moved according to the position of the objective lens. When the objective is located at an under- or over-focus position, the image is seen at the opposite side across the center, where it is formed by the objective at the in-focus position (Supplementary Fig. 1a). The center can be identified quickly as the middle point between two different slit images obtained by switching the incident angle of the laser 180 degrees. The side of the image corresponds to the z-direction of the shift of the objective from the in-focus position. The calculated deviation from the center is transmitted to a control unit to feedback-control the objective position. The gap difference between the in-focus positions determined by the device and human eyes can be adjusted by setting an offset value. Supplementary Fig. 1b shows the flow of the autofocusing process. This method, using two images with light from exactly opposite directions, is robust for variations in the sample condition (e.g., refractive index) that affect the optical path at the sample-coverslip interface and cause inaccurate focusing by conventional methods. The device can also be applied to normal microscopy, especially with high magnification. In Supplementary Fig. 1c, another method for switching the laser direction is introduced. A circular transparent plate with a thin circular coating (e.g., aluminum) forms thin light-nontransparent regions inside and outside each half of the circle. The laser illumination goes through the circles; therefore, when the plate rotates, the optical path is switched according to the rotational frequency, enabling illumination from opposite directions.

Single-molecule tracking

Single-molecule tracking was carried out on the acquired images to obtain the positions and brightness of fluorescent EGFR-mEGFP using commercial software (Auto Analysis Software, AAS, ZIDO, Japan). The first process of the tracking was to determine bright spots in the image by selecting square regions with 11×11 pixels beyond a threshold for cross-correlation between pixel values and the two-dimensional Gaussian distribution. Then, the spot region was fitted with the following function:

$$I\left(x, y; I_0, x_g, y_g, \sigma_A, a, b, I_{back}\right) = I_0\, exp\left[-\frac{(x - x_g)^2 + (y - y_g)^2}{2\sigma_A^2}\right] + a\left(x - x_g\right) + b\left(y - y_g\right) + I_{back}, \tag{2}$$

where x and y denote the pixel positions. The distribution of the pixel values was expressed as a Gaussian function with a peak intensity of I_O at the centroid, (x_g, y_g) and a variance of σ_A^2, plus a background with an inclination described by a and b above the offset intensity I_{back}. A single-molecule trajectory was generated by connecting the spots as follows: all possible connections between two spots at times t and $t-1$ with a center-to-center distance below 6 pixels were listed, and the shortest connection was selected. Trajectories outside the cell region determined by the AI-aided cell search algorithm were removed.

Molecular mobility analysis

The mobility of lateral diffusion was analyzed with the MSD calculated from the positions of the fluorescent spots with the following equation:

$$MSD(n\Delta t) = \left[\{x_i(n\Delta t + m\Delta t) - x_i(m\Delta t)\}^2 + \{y_i(n\Delta t + m\Delta t) - y_i(m\Delta t)\}^2\right]_{i, m} \tag{3}$$

Here, x_i and y_i represent the single-molecule position in the i-th track, n and m denote the frame number, Δt is the time interval between frames (33 ms), and $[]_{i,m}$ denotes the average over i tracks and m frames. For Fig. 1f and g, MSD at $\Delta t = 500$ ms was used. The dose-response curve (Fig. 1f) was plotted as the MSD ratio and fitted using the following equation to calculate the EC_{50}:

$$MSD = MSD_{\max} - \frac{MSD_{\max} - MSD_{\min}}{1 + \left(\frac{EC_{50}}{[L]}\right)^h}, \tag{4}$$

where MSD_{max} and MSD_{min} are the MSD ratios of the upper and lower boundaries, respectively, $[L]$ is the ligand (EGF) concentration, and h is the Hill coefficient. To display the dose-response curve in comparison with the phosphorylation level, the MSD ratio was converted as follows:

$$MSD_{converted} = \frac{MSD_{\max} - MSD}{MSD_{\max} - MSD_{\min}} \tag{5}$$

Compounds

The library of FDA-approved compounds (Selleck Chemicals, USA) was provided in 96-well plates from the Center for Supporting Drug Discovery and Life Science Research, Osaka University, in 2021. 3 µL of 1 mM compound in DMSO was dispensed in each well and diluted to 10 µM with DMEM before screening. The medium in 60 wells of the 96-well plate with cultured cells was replaced to the compound solution and incubated at 37 °C for 1 h. Both sides of the compound-treated wells (total 2×6 wells) were used for the positive and negative controls (with and without 10 µM gefitinib), respectively.

Single-molecule screening

For the compound screening, single-molecule imaging was executed on 20 cells before and 20 cells after EGF stimulation. 100 µL of 120 nM EGF was added to every well (final concentration, 60 nM). The MSD ratio was used to confirm the quality of the screening and select the hit compounds. For each plate, we calculated the Z'-factor using the MSD ratios of the wells with the positive (10 µM gefitinib in DMSO) and negative (DMSO only) controls. The MSD at Δt that provided the best Z'-factor in each well plate was used for Fig. 2c and at 167 ms for Fig. 2d and e. The average and SD of the MSD ratio of positive and negative controls were used to calculate the Z'-factor.

$$Z' = 1 - \frac{\left(3 \times SD_{positive}\right) + \left(3 \times SD_{negative}\right)}{Avg_{positive} - Avg_{negative}} \tag{6}$$

Here, Avg and SD respectively represent the averages and SD of the MSD for the positive and negative controls. In Fig. 2c, the MSD ratio for each compound was normalized to that of the negative control, and any compound with a ratio greater than the sum of the average and three-fold SD of the negative control was defined as a hit compound. For the compound-dose dependent assay shown in Fig. 2d and e, cells were treated with 100 µL of 10 µM, 1 µM, 0.1 µM, 0.01 µM, and 0.001 µM compound solution for 1 h before single-molecule imaging. Regardless of the EGF addition, when the MSD value was larger than half the difference of the MSD at the minimum and maximum compound concentration plus their SD, the compound was recognized as effective for EGFR.

Cell viability assay

A431, HeLa, Ba/F3 with and without EGFR expression, and CHO-K1 cells in 96-well plates (1860-096, Iwaki, Japan) were incubated in 10 µM compound solution at 37 °C for 72 h. Compound solutions for the A431, HeLa, and CHO-K1 cells were prepared by diluting stock solutions of compounds in HBSS. The solutions additionally contained EGF but no IL-3 for Ba/F3 cells expressing EGFR and only IL-3 for Ba/F3 cells not expressing EGFR. Then, the medium was replaced with 10 µL of Cell Counting Kit −8 (Dojindo, Japan) diluted in 100 µL HBSS. After 2 h of incubation, absorption of the medium was measured for each well with a wavelength of 450 nm using a plate reader (Infinite F50 Plus, Tecan, USA).

Western blotting

After the compound and/or EGF treatment, the cells were lyzed in SDS sample buffer. The lysate was electrophoresed on a 10% SDS-polyacrylamide precast gel (192-14961, SuperSep Ace, 10%, 17well, FUJIFILM Wako Pure Chemical, Japan) Then, the proteins were transferred to a 0.45 µm pore PVDF membrane (034-25663, ClearTrans PVDF Membrane, Hydrophobic, 0.45 µm, FUJIFILM Wako Pure Chemical, Japan) and reacted with antibodies against the following targets: EGFR (#4267, Cell signaling technology (CST), USA), phospho-EGFR (Tyr1068, #4267, CST, USA), AKT (#9272, CST, USA), phospho-AKT (Ser473, #4060, CST, USA), ERK1/2 (#9107, CST, USA), and phospho-ERK1/2 (Thr202/Try204, #9106, CST, USA). For chemiluminescent antibody detection, HRP-linked anti-rabbit IgG (#7074, CST, USA) and HRP-linked anti-mouse IgG (#7076, CST, USA) were used with ECL prime reagent (Cytiva, USA). The loading control containing proteins ranging from 37 to 250 kDa was obtained from the SDS gel stained with CBB. Quantification of the band densities was carried out using ImageJ software (NIH). Two squares were set such that one square was placed in the band and another square was far away from the band, and the difference in the average intensities of these regions was defined as the band intensity. The intensity of the anti-phosphorylated antibody was normalized to that of the anti-protein antibody. The phosphorylation level was calculated by dividing the normalized intensity of the

phosphorylated protein for each condition by that for 30 nM EGF without compound. The EGF dose-response curve was fitted with the Hill equation as follows:

$$phosphorylation = \min - \frac{\max - \min}{1 + \left(\frac{EC_{50}}{[L]}\right)^h}. \qquad (7)$$

Here, h indicates the Hill coefficient, max, and min denote upper and lower bounds, respectively, and $[L]$ is the concentration of the ligand, EGF. The protein expression amount was calculated by normalizing the intensity of the protein for each condition by that of the loading control.

Internalization assay

For quantification of the internalization (Fig. 4d and e), CHO-K1 cells expressing EGFR-mEGFP in a 96-well plate were treated in compound solution for 1 h. The compound solutions were the same as those used in the experiment above. After the compound treatment, timelapse single-molecule images (Fig. 4d) were acquired by AiSIS at the same positions in a well every 10 min. For verteporfin, which showed rapid photobleaching of EGFR-mEGFP as a photophysical effect induced by repetitive laser irradiation, the images were obtained at the same positions at only two-time points (0 min and 20, 40, 60, or 80 min) to minimize the effect. In the obtained images, the average brightness was measured for circled regions of interest (ROI) within a cell and outside the cell (background). The difference in the brightness between these regions was calculated for each time point and normalized to the value at time 0 (Fig. 4e). To consider the effect of fluorescence bleaching caused by repetitive irradiation by the laser, timelapse images of the cells without compound treatment were acquired and analyzed by the same method.

Immunofluorescence microscopy

The compound treatment of A431 and HeLa cells cultured in 24-well plates was carried out in 10 μM solutions for 1 hour at 37°C after the cells were incubated in DMEM without FBS for 6 hours. Subsequently, the compounds were washed out with HBSS, and the cells were fixed with 4% PFA for 30 min at 4 °C and solubilized with 0.5% Triton X100 in HBSS at room temperature, followed by washing with HBSS three times and left at 4 °C overnight. After the blocking process with HBSS containing 2% BSA for 15 min, 1:300-diluted anti-EGFR antibody (#4267, CST, USA) or 1:10,000-diluted anti-caveolin antibody (#3267 T, CST, USA) was added as the primary antibody for 1 hour at room temperature. The cells were washed with HBSS three times and labeled with 1:1000 anti-IgG antibody conjugated with Alexa 488 or Alexa 647 (#A-11034 or #A-21244, respectively, Invitrogen, USA) for 1 h at room temperature. The nucleus was fluorescently labeled with 0.05% NucSpot Live 650 (Biotium, USA) for 30 min at room temperature. Observation of the samples was done by confocal microscopy (Nikon A1) with a 20X objective lens (Nikon PalnApo) operated with NIS elements software (Nikon). The preparation process for EGFR-transfected Ba/F3 cells was almost the same as that for other cells, except that floating cells in Eppendorf tubes were centrifuged with $800 \times g$ for 2 min to replace the supernatant after every step. For the observation, the cells were suspended in HBSS in a 96-well plate. The obtained images were analyzed by quantifying the fluorescence intensity of the plasma membrane and cytoplasm to calculate the ratio of EGFR in these regions. The regions of the plasma membrane and cytoplasm were identified as the area within 5 pixels inside the cell boundary, which was determined with Cellpose 3.0, and the other pixels within the cell, respectively. The average fluorescence intensities of the plasma membrane (F_{mem}), the cytoplasm (F_{cyt}), and background area (F_{bck}) where no cells existed were obtained to calculate the ratio, $I_{mem}/$

$I_{cyt} = (F_{mem} - F_{bck})/(F_{cyt} - F_{bck})$, as the extent of internalization. In addition, the decrease in total EGFR in a cell due to degradation was taken into account as the intensity ratio of the whole cell with to without compound treatment $\alpha = (F_{drug} - F_{bck})/(F_{ctrl} - F_{bck})$. The product of this ratio ($\alpha \cdot I_{mem}/I_{cyt}$) includes both the internalization and degradation effects of a compound, which correspond to the fluorescence change in the obtained image. The calculations were performed using a custom-made program written in Python 3.8.18.

Reporting summary

Further information on research design is available in the Nature Portfolio Reporting Summary linked to this article.

Data availability

Source data are provided with this paper. All other data supporting the findings of this study are available in the Supplementary Information file and from the corresponding author upon request.

Code availability

All Python and ImageJ scripts supporting the findings of this paper are available upon reasonable request. The code used in this paper is deposited in the GitHub repository at https://github.com/d-watana/Single-Molecule-Imaging-Data-Analysis.

References

1. Santos, R. et al. A comprehensive map of molecular drug targets. *Nat. Rev. Drug Discov.* **16**, 19–34 (2016).
2. Hopkins, A. L. & Groom, C. R. The druggable genome. *Nat. Rev. Drug Discov.* **1**, 727–730 (2002).
3. Vasaikar, S., Bhatia, P., Bhatia, P. G. & Yaiw, K. C. Complementary approaches to existing target based drug discovery for identifying novel drug targets. *Biomedicines* **4**, 27 (2016).
4. Kovacs, T., Zakany, F. & Nagy, P. It takes more than two to tango: complex, hierarchal, and membrane-modulated interactions in the regulation of receptor tyrosine kinases. *Cancers* **14**, 944 (2022).
5. Normanno, N., Maiello, M. R. & Luca, A. D. E. Epidermal growth factor receptor tyrosine kinase inhibitors (EGFR-TKIs): simple drugs with a complex mechanism of action? *J. Cell. Physiol.* **19**, 13–19 (2002).
6. Roengvoraphoj, M., Tsongalis, G. J., Dragnev, K. H. & Rigas, J. R. Epidermal growth factor receptor tyrosine kinase inhibitors as initial therapy for non-small cell lung cancer: Focus on epidermal growth factor receptor mutation testing and mutation-positive patients. *Cancer Treat. Rev.* **39**, 839–850 (2013).
7. Chiba, M. et al. Efficacy of irreversible EGFR-TKIs for the uncommon secondary resistant EGFR mutations L747S, D761Y, and T854A. *BMC Cancer* **17**, 281 (2017).
8. Du, X. et al. Acquired resistance to third-generation EGFR-TKIs and emerging next-generation EGFR inhibitors Acquired resistance to third-generation EGFR-TKIs and emerging next-generation EGFR inhibitors. *Innovation* **2**, 100103 (2021).
9. Gao, J., Jian, J., Jiang, Z. & Van Schepdael, A. Screening assays for tyrosine kinase inhibitors: a review. *J. Pharm. Biomed. Anal.* **223**, 115166 (2023).
10. Wee, P. & Wang, Z. Epidermal growth factor receptor cell proliferation signaling pathways. *Cancers* **9**, 52 (2017).
11. Peters, C. et al. Characterization of a new molecule capable of inhibiting several steps of the amyloid cascade in Alzheimer's disease. *Neurobiol. Dis.* **141**, 104938 (2020).
12. Sako, Y., Minoguchi, S. & Yanagida, T. Single-molecule imaging of EGFR signalling on the surface of living cells. *Nat. Cell Biol.* **2**, 168–172 (2000).
13. Ueda, M., Sako, Y., Tanaka, T., Devreotes, P. & Yanagida, T. Single-molecule analysis of chemotactic signaling in Dictyostelium cells. *Science* **294**, 864–867 (2001).

14. Iino, R., Koyama, I. & Kusumi, A. Single molecule imaging of green fluorescent proteins in living cells: E-cadherin forms oligomers on the free cell surface. *Biophys. J.* **80**, 2667–2677 (2001).

15. Hiroshima, M. et al. Transient acceleration of epidermal growth factor receptor dynamics produces higher-order signaling clusters. *J. Mol. Biol.* **430**, 1386–1401 (2018).

16. Hiroshima, M., Saeki, Y., Okada-Hatakeyama, M. & Sako, Y. Dynamically varying interactions between heregulin and ErbB proteins detected by single-molecule analysis in living cells. *Proc. Natl Acad. Sci. USA* **109**, 13984–13989 (2012).

17. Clarke, D. T. & Martin-Fernandez, M. L. A brief history of single-particle tracking of the epidermal growth factor receptor. *Methods Protoc.* **2**, 12 (2019).

18. Byeon, H. K. Beyond EGFR inhibition: multilateral combat strategies to stop the progression of head and neck cancer. *Exp. Mol. Med.* **51**, 8 (2019).

19. Gamble, M. C. et al. Mu-opioid receptor and receptor tyrosine kinase crosstalk: Implications in mechanisms of opioid tolerance, reduced analgesia to neuropathic pain, dependence, and reward. *Front. Syst. Neurosci.* **16**, 1059089 (2022).

20. Yasui, M., Hiroshima, M., Kozuka, J., Sako, Y. & Ueda, M. Automated single-molecule imaging in living cells. *Nat. Commun.* **9**, 3061 (2018).

21. Yasui, M., Hiroshima, M. & Ueda, M. United States Patent: 11567293. (2023).

22. Abourehab, M. A. S., Alqahtani, A. M., Gouda, B. G. M. Y. & Gouda, A. M. Globally approved EGFR inhibitors: insights into their syntheses, target kinases, biological activities, receptor interactions, and metabolism. *Molecules* **26**, 6677 (2021).

23. Falco et al. Ponatinib (AP24534) is a novel potent inhibitor of oncogenic RET mutants associated with thyroid cancer. *J. Clin. Endocrinol. Metab.* **98**, 811–819 (2013).

24. Joseph, R. E. et al. Differential impact of BTK active site inhibitors on the conformational state of full-length BTK. *eLife* **9**, e60470 (2020).

25. Lehmann, M. et al. Activity of topoisomerase inhibitors daunorubicin, idarubicin, and aclarubicin in the drosophila somatic mutation and recombination test. *Environ. Mol. Mutagen.* **257**, 250–257 (2004).

26. Grainger, J. D. Eltrombopag for the treatment of aplastic anemia: current perspectives. *Drug Des. Dev. Ther.* **10**, 2833–2843 (2016).

27. Carlile, G. W. et al. The NSAID glafenine rescues class 2 CFTR mutants via cyclooxygenase 2 inhibition of the arachidonic acid pathway. *Sci. Rep.* **12**, 4595 (2022).

28. Guevremont, C., Jeldres, C., Perrotte, P. & Karakiewicz, P. I. Sorafenib in the management of metastatic renal cell carcinoma. *Curr. Oncol.* **16**, S27–S32 (2009).

29. Kantarjian, H. M. et al. Nilotinib is effective in patients with chronic myeloid leukemia in chronic phase after imatinib resistance or intolerance: 24-month follow-up results. *Blood* **117**, 1141–1145 (2011).

30. Borodoker, N. et al. Verteporfin infusion-associated pain. *Am. J. Ophthalmol.* **133**, 211–214 (2002).

31. Janmaat, M. L., Kruyt, F. A. E., Rodriguez, J. A. & Giaccone, G. Response to epidermal growth factor receptor inhibitors in non-small cell lung cancer cells: Limited antiproliferative effects and absence of apoptosis associated with persistent activity of extracellular signal-regulated kinase or Akt kinase pathways. *Clin. Cancer Res.* **9**, 2316–2326 (2003).

32. Walker, F. et al. Activation of the ras/mitogen-activated protein kinase pathway by kinase-defective epidermal growth factor receptors results in cell survival but not proliferation. *Mol. Cell Biol*. **18**, 7192–7204 (1998).

33. Okada, T., Miyagi, H., Sako, Y., Hiroshima, M. & Mochizuki, A. Origin of diverse phosphorylation patterns in the ERBB system. *Biophys. J.* **121**, 1–11 (2021).

34. Giocanti, N., Hennequin, C., Rouillard, D., Defrance, R. & Favaudon, V. Additive interaction of gefitinib ('Iressa', ZD1839) and ionising radiation in human tumour cells in vitro. *Br. J. Cancer* **91**, 2026–2033 (2004).

35. Sharma, A. et al. On-water NiFe2O4 nanoparticle-catalyzed one-pot synthesis of biofunctionalized pyrimidine-thiazole derivatives: In silico binding affinity and in vitro anticancer activity studies. *ChemistrySelect* **3**, 11012–11019 (2018).

36. Morita, K. et al. In situ synthesis of an anticancer peptide amphiphile using tyrosine kinase overexpressed in cancer cells. *JACS Au* **2**, 2023–2028 (2022).

37. Mcswiggen, D. T. et al. A high-throughput platform for single-molecule tracking identifies drug interaction and cellular mechanisms. *eLife* **12**, RP93183 (2024).

38. de Laurentiis, A., Donovan, L. & Arcaro, A. Lipid rafts and caveolae in signaling by growth factor receptors. *Open Biochem. J.* **1**, 12–32 (2007).

39. Bourseau-Guilmain, E. et al. Hypoxia regulates global membrane protein endocytosis through caveolin-1 in cancer cells. *Nat. Commun.* **7**, 11371 (2016).

40. Jo, U. et al. EGFR endocytosis is a novel therapeutic target in lung cancer with wild-type EGFR. *Oncotarget* **5**, 1265–1278 (2014).

41. Heppner, D. E. & van der Vliet, A. Redox-dependent regulation of epidermal growth factor receptor signaling. *Redox Biol.* **8**, 24–27 (2016).

42. Kim, S. Y. et al. Effects of clioquinol analogues on the hypoxia-inducible factor pathway and intracelullar mobilization of metal ions. *Biol. Pharm. Bull.* **35**, 2160–2169 (2012).

43. Wang, Y. et al. Hypoxia promotes ligand-independent EGF receptor signaling via hypoxia-inducible factor-mediated upregulation of caveolin-1. *Proc. Natl Acad. Sci. USA* **109**, 4892–4897 (2012).

44. Wen, S. Y. et al. Doxorubicin induced ROS-dependent HIF1α activation mediates blockage of IGF1R survival signaling by IGFBP3 promotes cardiac apoptosis. *Aging* **15**, 164–178 (2023).

45. Wang, H., Jin, H. & Rapraeger, A. C. Syndecan-1 and syndecan-4 capture epidermal growth factor receptor family members and the α3β1 integrin via binding sites in their ectodomains: novel synstatins prevent kinase capture and inhibitα6β4-integrindependent epithelial cell motility. *J. Biol. Chem.* **290**, 26103–26113 (2015).

46. Alves, A. C. et al. A biophysical approach to daunorubicin interaction with model membranes: relevance for the drug's biological activity. *J. R. Soc. Interface* **14**, 20170408 (2017).

47. Matthews, E. E. et al. Thrombopoietin receptor activation: transmembrane helix dimerization, rotation, and allosteric modulation. *FASEB J.* **25**, 2234–2244 (2011).

48. Stewart, E. L., Tan, S. Z., Liu, G. & Tsao, M. Known and putative mechanisms of resistance to EGFR targeted therapies in NSCLC patients with EGFR. *Transl. Lung Cancer Res.* **4**, 67–81 (2015).

49. Maeda, R., Sato, T., Okamoto, K., Yanagawa, M. & Sako, Y. Lipid-protein interplay in dimerization of juxtamembrane domains of epidermal growth factor receptor. *Biophys. J.* **114**, 893–903 (2018).

50. Yoshimura, A., Longmore, G. & Lodish, H. F. Point mutation in the exoplasmic domain of the erythropoietin receptor resulting in hormone-independent activation and tumorigenicity. *Nature* **348**, 647–649 (1990).

51. Gotoh, N., Tojo, A., Hino, M., Yazaki, Y. & Shibuya, M. A highly conserved tyrosine residue at codon 845 within the kinase domain is not required for the transforming activity of human epidermal growth factor receptor. *Biochem. Biophys. Res. Commun.* **186**, 768–774 (1992).

Acknowledgements

Author contributions

Conceptualization: M.H. and M.U. Methodology: D.W., M.Y., and M.H. Investigation: D.W. and M.H. Funding acquisition: M.H. and M.U. Supervision: M.U. Writing—original draft: D.W., M.H., and M.U. Writing—review & editing: M.H. and M.U.

Competing interests

The authors declare no competing interests.

Additional information

Supplementary information The online version contains supplementary material available at https://doi.org/10.1038/s41467-024-53432-w.

Correspondence and requests for materials should be addressed to Michio Hiroshima or Masahiro Ueda.

Peer review information *Nature Communications* thanks David E Heppner and the other anonymous reviewer(s) for their contribution to the peer review of this work. A peer review file is available.

Reprints and permissions information is available at http://www.nature.com/reprints

Publisher's note Springer Nature remains neutral with regard to jurisdictional claims in published maps and institutional affiliations.